Influence of Copper Addition in AlSi7MgCu Alloy on Microstructure Development and Tensile Strength Improvement

Stanić, Davor; Zovko Brodarac, Zdenka; Li, Letian

Source / Izvornik: **Metals, 2020, 10, 1 - 16**

Journal article, Published version
Rad u časopisu, Objavljena verzija rada (izdavačev PDF)

https://doi.org/10.3390/met10121623

Permanent link / Trajna poveznica: https://urn.nsk.hr/urn:nbn:hr:115:217591

metals

MDPI

Article

Influence of Copper Addition in AlSi7MgCu Alloy on Microstructure Development and Tensile Strength Improvement

Davor Stanić [1], Zdenka Zovko Brodarac [2,*] and Letian Li [3]

[1] CIMOS-P.P.C. Buzet, d.o.o., Most 24, 52420 Buzet, Croatia; Davor.Stanic@cimos.eu
[2] Department for Process Metallurgy, Faculty of Metallurgy, University of Zagreb, Aleja Narodnih Heroja 3, 44103 Sisak, Croatia
[3] Materials & Structural Analysis Division, Thermo Fisher Scientific, Europe NanoPort, Achtseweg Noord 5, 5651 GG Eindhoven, The Netherlands; letian.li@thermofisher.com
* Correspondence: zovko@simet.hr; Tel.: +385-98-595-755

Received: 27 October 2020; Accepted: 26 November 2020; Published: 2 December 2020

Abstract: Commercial AlSi7Mg alloy represents the usual choice for complex geometry casting production. The market imperative to improve mechanical properties imposed the design of new chemical composition of AlSi7MgCu alloy with high content of Cu (up to 1.435 wt.%). This represents a challenge in order to achieve advanced properties. The interaction of a number of alloying (Si, Mg, Cu) and trace elements (Fe, Mn) influenced a wide range of complex reactions occurring and therefore leading to intermetallic phase precipitation. The characterization of novel chemical composition interaction and its solidification sequence was achieved by modelling an equilibrium phase diagram, simultaneously performing both thermal analysis and metallographic investigations. Copper influence was indicated in the whole solidification process starting with infiltration in modified Chinese script phase $Al_{15}(Fe,Mn,Cu)_3Si_2$, beside common intermetallic Al_5FeSi. Copper addition encourages formation of compact complex intermetallic phases $Al_5Cu_2Mg_8Si_6$ and $Al_8(Fe,Mn,Cu)Mg_3Si_6$. Solidification ended with secondary eutectic $\alpha_{Al} + Al_2Cu + \beta_{Si}$. Microstructure investigation allows volume reconstruction of the microstructure and distribution of particular phases. Chemical compositions enriched in copper content and developed microstructural constituent through solidification sequence of AlSi7MgCu alloy contribute to a significant increase in mechanical properties already in an as-cast state.

Keywords: AlSi7MgCu alloy; copper; microstructure; solidification sequence; mechanical properties

1. Introduction

High market demands related to material quality and properties strongly influence redesigning of common safety loaded aluminum alloy castings. The quality of aluminum components and associated obtained mechanical properties are strongly dependent on the casting process and parameters, as well as on the chemical composition. Therefore, the redesigning of chemical composition of high-strength aluminum alloys becomes significant for safety critical structural components in automotive industry.

Common AlSi7Mg alloy represents a frequent choice for complex geometry castings with high properties demand due to excellent castability and favorable relation between strength and weight, especially in the heat-treated state. Synergy of alloying and trace elements contributes to the wide range of intermetallic phase evolution [1–6]. The content of secondary alloying elements (Mg, Cu) significantly changes the solidification path of the Al-Si alloy [7–19]. The addition of secondary elements, melt treatment, and solidification conditions have a synergy effect on the crystallization kinetic and therefore on the properties' development as well [20–26]. Intermetallic phase development could be attributed to the constitutional undercooling and its equilibrium partition coefficient, *k*. When compared

to existing solid phase, bulk liquid becomes enriched in solute elements and can originate different intermetallic phases and microsegregation during solidification process. Coexistence of number of complex intermetallic phases and their solidification sequence in correlation to cooling/solidification conditions influence on achieved final properties.

The solidification sequence of hypoeutectic AlSi7Mg alloys begins with development of primary aluminum dendrites αAl and formation of dendritic network, followed by the eutectic reaction (α_{Al} + β_{Si}) on the primary grains α_{Al} or independently on a present nucleant rich in iron and/or other impurities with different crystallographic orientation [8]. The primary and most important alloying element in conventional AlSi7Mg alloy is Si, which is characterized by high fluidity and reduction in shrinkage, followed by Mg, responsible for strength increase especially in heat-treated state [8–11].

Magnesium addition up to a 0.7 wt.% has a strengthening effect through the precipitation of α_{Al} + Mg_2Si eutectic phase and/or Mg-rich intermetallic with other alloying elements mostly due to transformation of the deleterious Al_5FeSi platelets into a ramified morphology with stoichiometry $Al_8Mg_3FeSi_6$. [9,12,13]. High Mg content comprehends to the Al_8Mg_5 phase precipitation at the grain boundaries [14]. The yield strength, tensile strength, and elongation of the as-cast Al-Si-Mg alloys can vary with the Mg content [15]. The yield strength increases with increasing of Mg content, although no significant influence with increasing the Mg_2Si phase content has been determined. Conversely, the elongation decreases with an increase in the Mg and Mg_2Si ratio [15].

Additionally, Cu is a frequent addition as a secondary alloying element in order to increase the strength of cast alloys, especially when heat treatment is applied. In Al-Si alloys, Cu is usually added in levels between 1.5–3.5 wt.%, thus forming the intermetallic phase Al_2Cu [16–18]. Copper significantly decreases the solidus and eutectic temperature of an alloy. Therefore, the copper enlarges the solidification interval of an alloy and facilitates the condition of porosity formation [19,26,27]. The literature survey reveals a number of investigations related to the influence of alloying elements on the AlSi7Mg alloy properties [28–30]. A correlation of equilibrium phase diagram modelling, thermal analysis results, and microconstituent identification allows the determination of the thermodynamic stability of an alloy and its behavior [5,31–34]. The conventional AlSi7Mg alloy, corresponding to numerous standards (EN 1706, IDM 4234) [35,36], has been investigated previously [37]. Requested chemical composition is indicated in Table 1.

Table 1. Chemical composition of AlSi7Mg alloy [35].

Chemical Element	wt.%	Si	Fe	Cu	Mn	Mg	Zn	Ti	Ni	Pb	Bal.
EN AC 42000	min.	6.5	-	-	-	0.20	-	0.05	-	-	-
	max.	7.5	0.55	0.20	0.35	0.65	0.15	0.25	0.15	0.15	0.15

Automotive producers' standard [36] narrows the requested content interval of particular elements such as Mg, while at the same time, it widens the Fe content range, whose phases in corresponding morphologies can contribute to the aluminum alloys strength increase. Demand for mechanical properties of AlSi7Mg alloy, in particular yield strength ($R_{p0.2}$), tensile strength (R_m), and elongation relating to 50 mm test length for separately cast samples in as-cast state (A_{50}), shown in Table 2, is strictly prescribed by norm (EN 1706) [35,38].

Table 2. Requested mechanical properties of AlSi7Mg alloy separately cast samples in as-cast state [35].

	$R_{p0.2}$/MPa	R_m/MPa	A_{50}/%
EN AC 42000	90	170	2.5

An innovative approach in this investigation was pointed into the redesigning the chemical composition of common AlSi7Mg alloy in order to improve its mechanical properties. With this aim, an extra addition of Cu (1.435 wt.%) as a secondary alloying element, has been added. The hypothesis

of this investigation was that higher content of Cu will modify the solidification sequence of innovative AlSi7MgCu alloy due to numerous additional interactions. The consequence of presumed interactions reflects in the development of complex but morphologically favorable intermetallic phases [39,40]. Innovative approach obtained with higher Cu content in AlSi7MgCu alloy reveals an improvement in the requested tensile strength already in as-cast state.

2. Materials and Methods

Characterization of solidification sequence of the newly designed AlSi7MgCu alloy has been performed through the correlation of equilibrium phase diagram modelling, the results of simultaneous thermal analysis, XRD analysis, and microstructural analysis.

Thermodynamic calculations of equilibrium and Scheil–Gulliver non-equilibrium phase diagram of AlSi7MgCu alloy have been performed by Thermo-Calc software TCW 5.0 (Thermo-Calc Software, Stockholm, Sweden), with database TTAL7.

The newly designed AlSi7MgCu alloy melt was prepared in an induction furnace ABB IMTK 2000 (ABP Induction Systems GmbH, Dortmund, Germany). Charge material and return material ratio was 1:1. After melt preparation (770 ± 5 °C), degassing was performed with the nitrogen (N_2) using an MTS 1500—Foseco melt treatment system (Vesuvius GmbH - Foseco Foundry Division, Borken, Germany). Melt treatment consists of inoculation with AlTi5B master alloy and modification with AlSr10 master alloy. Chemical composition analysis was performed using optical emission spectrometer ARL-3460 (Thermo Scientific^{TM}, Waltham, MA, USA). Uncertainty of measurements obtained by certification with reference material has been indicated in results for every particular element.

Metallographic investigation samples were prepared by using standard metallographic preparation procedure by grinding and polishing, followed by etching in 0.5% HF. Metallographic analyses cover optical microscopy analysis (Olympus GX 51; Olympus Europa SE & Co. KG, Hamburg, Germany) and microstructural investigations using a standard method with a scanning electron microscope equipped with an energy dispersive X-ray spectrometer (SEM-EDS, Tescan Vega TS 5136 MM; TESCAN ORSAY HOLDING, a.s., Brno, Czech Republic). Standard SEM-EDS analysis allows mapping analysis of the characteristic region using EDS detector. Focused ion beam scanning electron microscopes (FIB-SEM, Helios NanoLab G4 DualBeamTM; Thermo Fisher Scientific, Materials & Structural Analysis Division, Hillsboro, OR, USA) were equipped with 3D slicing/imaging technology. The 3D data were reconstructed using Avizo software, and analysis was subsequently performed in order to visualize 3D distribution of intermetallic phases in the corresponding region of interest. Slices with 15 nm thickness, obtained by FIB milling ($V = 19 \times 12 \times 12$ μm^3), were analyzed. The number of SE images was analyzed by FEI AVIZO software in order to obtain 3D reconstruction of phases' distribution. EDS analysis was applied in order to identify chemical composition of particular phases and to predict the resulted stoichiometry in correlation to corresponding morphologies.

Transformation temperatures were obtained by simultaneous thermal analysis, differential scanning calorimetry/thermogravimetry, with instrument STA DSC/TG, NETZSCH Jupiter 449 F1 (NETZSCH Holding, Selb, Germany). Temperature and sensitivity calibration files were created with measurements of 8 different pure materials: In, Sn, Bi, Pb, Zn, Al, Ag, and Ni. The resolution of DSC instrument was 1 μm and temperature resolution 0.001 K. Base line was determined with alumina pans. Dynamic measurements were performed in temperature interval from 25 to 710 °C, in argon atmosphere, with a heating/cooling rate of 10 °C/min. Measurements were repeated 2 times, and the results of the second measurement were presented as referent obtained values.

X-ray diffraction (XRD) technique was used for additional identification of the phases present in investigated alloys. PANalytical X'Pert PRO diffractometer (Malvern Panalytical Ltd, Malvern, UK) with non-monochromated X-rays produced by Empyrean Cu anode tube operating at 45 kV and 40 mA were used in this investigation.

Mechanical tensile properties investigations were performed on testing machine MTS 810 (MTS, Eden Prairie, Minneapolis, MN, USA), at room temperature T = 20 °C in accordance with

EN 10002-1:1998 [38]. Five samples for tensile testing were prepared with a diameter of 5 mm and a measuring length of 38.24 mm, as presented in Figure 1.

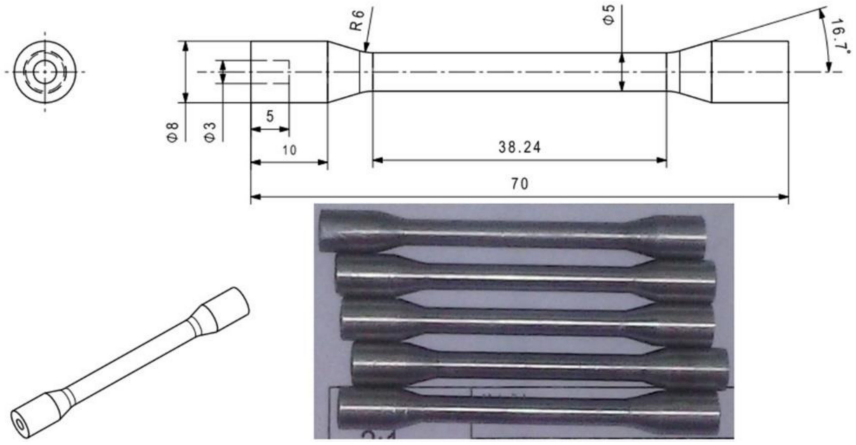

Figure 1. Samples for tensile strength testing (dimensions in mm).

3. Results

New chemical composition of AlSi7MgCu alloy with the extra addition of copper has been designed and compared with those prescribed by EN norm [35] indicated in Table 1 and previously investigated conventional AlSi7Mg alloy [38], as shown in Table 3. Chemical composition analysis was performed using optical emission spectrometry with indicated measurement uncertainty.

Table 3. The chemical compositions of AlSi7MgCu/AlSi7Mg alloys.

Element, wt.%	Si	Fe	Cu	Mn	Mg	Ti	Sr
AlSi7MgCu	7.527 ± 0.15	0.235 ± 0.019	1.435 ± 0.04	0.076 ± 0.009	0.348 ± 0.009	0.147 ± 0.0021	0.0223 ± 0.005
AlSi7Mg	7.008 ± 0.15	0.101 ± 0.019	0.130 ± 0.04	0.010 ± 0.009	0.320 ± 0.009	0.139 ± 0.0021	0.0121 ± 0.005

Both alloys, commercial AlSi7Mg and the new AlSi7MgCu, comply with the EN 42000 AC standard for AlSi7Mg alloy relating to the content of the base alloying elements (Si and Mg) and trace elements such as Fe and Mn. Deviation has been implemented with significant increase in Cu content.

Thermodynamic calculation of the newly designed AlSi7MgCu alloy by TCW 5.0 program resulted in equilibrium and Scheil–Gulliver non-equilibrium phase diagram. Interaction of alloying and trace elements reveals a wide range of intermetallic phases. Calculation of AlSi7MgCu alloy solidification sequence is shown in Figure 2.

Equilibrium condition calculation enabled an overview of stable equilibrium phases in aluminum corner of phase diagram. Non-equilibrium calculation revealed solidification sequence of AlSi7MgCu alloy with temperature stability of present phases. It reveals narrow solidification interval of $\Delta T_{L\text{-}S}$ = 96.4 °C. The calculated solidification sequence is as follows:

(1) 606.5 °C $L \rightarrow L_1 + \alpha_{Al}$
(2) 569.0 °C $L_1 \rightarrow L_2 + \beta_{Si}$
(3) 564.4 °C $L_2 \rightarrow L_3 + (\alpha_{Al} + \beta_{Si})$
(4) 537.4 °C $L_3 \rightarrow L_4 + Al_5FeSi$
(5) 537.4 °C $L_4 \rightarrow L_5 + Al_8FeMg_3Si_6$
(6) 528.0 °C $L_5 \rightarrow L_6 + Al_5Cu_2Mg_8Si_6$
(7) 510.1 °C $L_6 \rightarrow L_7 + Al_7Cu_2Mg$
(8) 510.1 °C $L_7 \rightarrow Al_2Cu$

Microstructure of AlSi7MgCu alloy was investigated using optical microscopy to get an overview of microstructure development, as shown in Figure 3.

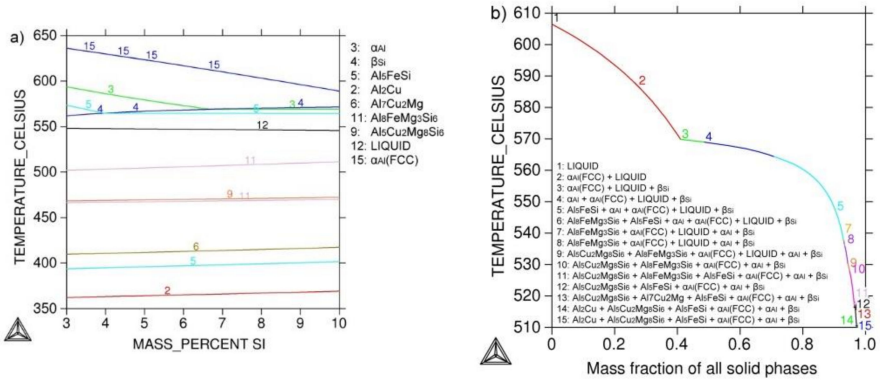

Figure 2. Modelling of solidification sequence of AlSi7MgCu alloy: (**a**) part of equilibrium Al-Si phase diagram, (**b**) Scheil–Gulliver non-equilibrium phase diagram.

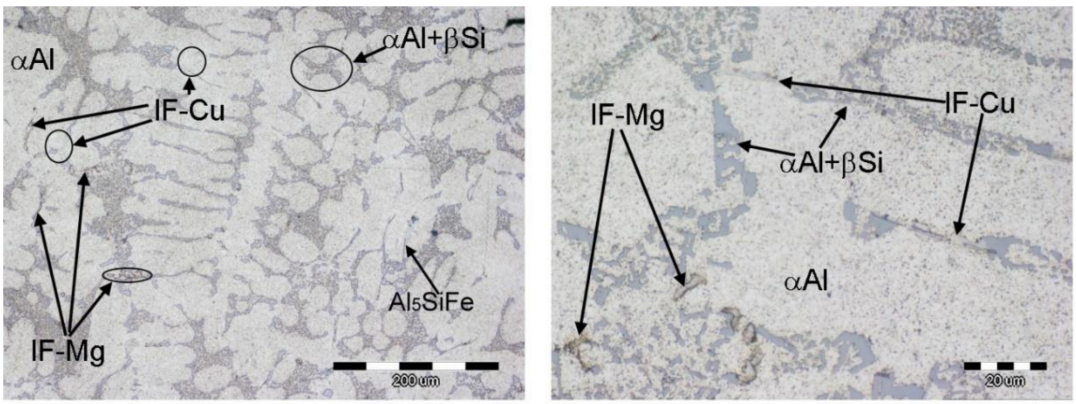

Figure 3. Micrographs of AlSi7MgCu alloy obtained by optical microscopy at different magnification: (**a**) 200×; (**b**) 1000×.

Identification of present phases at micrographs was performed using visual assessment to its morphologies and comparison with literature survey of similar alloys. A smaller magnification reveals uniform distribution of primary dendritic network surrounded by evenly distributed eutectic cells. Higher magnification indicates rougher and broken dendritic branches dotted with Fe-bearing intermetallic phases with needle-like morphology (Al_5SiFe) and Chinese script ($Al_{15}(Fe,Mn)_3Si_2$); light-grey to white coarse intermetallic phases, which correspond to Cu-bearing phases (IF-Cu) in interdendritic spaces and at grain boundaries; and fine dark intermetallic phases, which correspond to Mg-bearing phases (IF-Mg) placed at grain boundaries. High magnification micrographs also reveal mixed morphology of main eutectic (α_{Al} + β_{Si}), both fiber and lamella. On the base of visual recognition of particular phases and their micro-locations, it can be stated that a modelled solidifying sequence has been followed. The IF-Cu phases seem to occur through the whole solidification sequence—near the high-temperature needle-like Fe-bearing phases, in interdendritic spaces and at grain boundaries—whereas the IF-Mg phases occur only at the grain boundaries as an intermetallic phase in combination with Fe, Mn, and/or Cu.

EDS mapping analysis of AlSi7MgCu alloy sample is performed in order to determine the distribution of significant chemical elements and their mutual interaction. The elements of interest were Al, Si, Fe, Mn, Mg, and Cu, as shown in Figure 4.

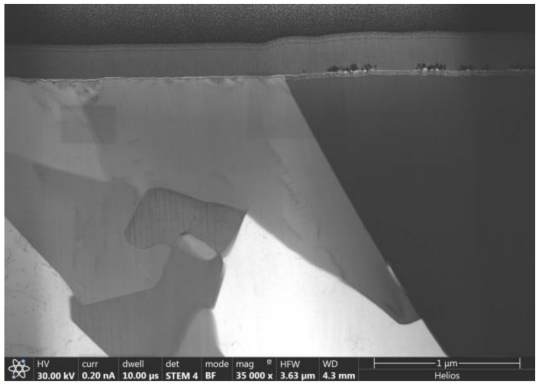

(**a**)

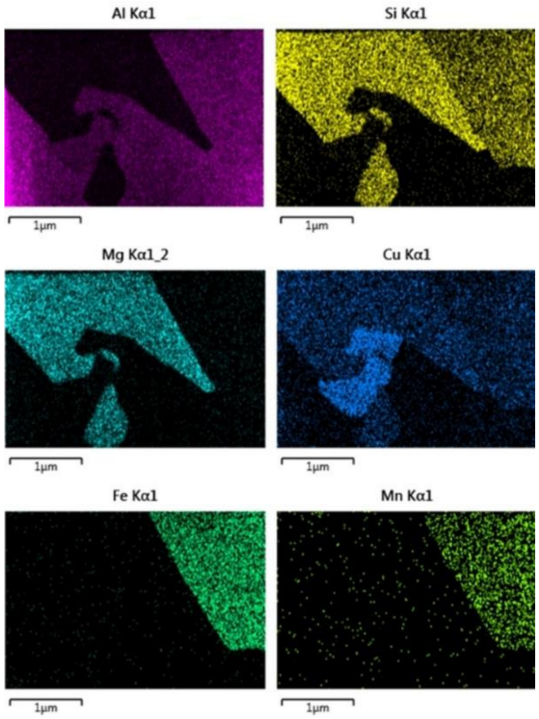

(**b**)

Figure 4. EDS mapping analysis of AlSi7MgCu alloy: (**a**) STEM image [41], (**b**) corresponding EDS elemental maps of Al, Si, Mg [41], Cu [41], Fe [41], and Mn [41]. (Copyright 2019 by The Minerals, Metals & Materials Society. Used with permission.)

EDS analysis reveals strong interaction of present elements forming following systems: Al-Fe-Mn-Cu-Si, Al-Mg-Cu-Si, Al-Cu, and Mg-Si. The obtained results indicate that Mn and non-equilibrium solidification played an important role in formation of $Al_{15}(Fe,Mn)_3Si_2$ phase instead of Al_5FeSi, as predicted in calculation of the equilibrium phase diagram. Additionally, Cu distribution proofs its infiltration in high-temperature intermetallic phase with modified chemical composition corresponding to the Al-(Fe-Mn-Cu)-Si system.

Since data acquired from the sample surface do not provide information about the phases' size, distribution and interaction, FIB-SEM analysis on 782 slices was applied. The obtained SE images enable 3D reconstruction of microstructure and distribution of each phase. A FIB-SEM slice-and-view study of three-dimensional phase distribution in AlSi7MgCu alloy is shown in Figure 5.

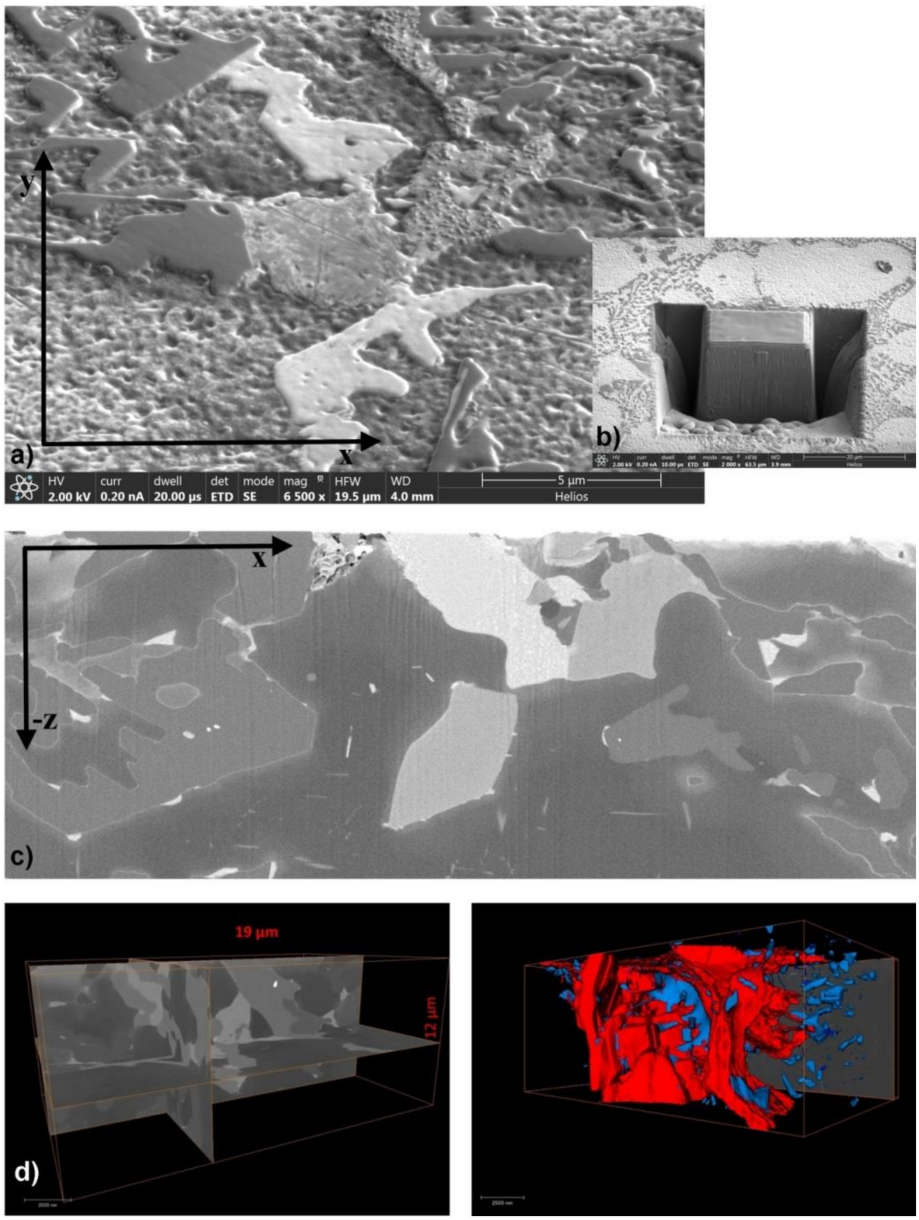

Figure 5. Focused ion beam scanning electron microscopes (FIB/SEM) tomography of AlSi7MgCu alloy: (**a**) SE image of the surface, (**b**) SE image of the trench prior to FIB/SEM, (**c**) orthoslice example of the x-(-z) imaging plane, (**d**) 3D distribution and shape of the Al-Si-Mg-Cu (red) and Al-(Fe-Mn-Cu)-Si (blue). Animation is available as a Supplementary Material Video S1.

Among all systems previously identified by regular mapping analysis, volume distribution of phases of interest on the base, the Al-Si-Mg-Cu (red) and Al-(Fe-Mn-Cu)-Si (blue) systems enable visualization of their distribution and interaction. Orthoslices in the order of appearance of each of the imaging plane provide an insight in the solidification sequence and visual estimation of phases' coherency and/or congruency. The dense arrangement of present phases, their size, and their distribution determine the order of appearance. First to appear is dendrite network (α-Al), followed by fine, but ramified Al-(Fe-Mn-Cu)-Si phases and main eutectic. The bulk of the volume was filled with Al-Si-Mg-Cu phase and other intermetallic phases on the base of Al-Fe-Mg-Si, Al-Cu-Mg, and Al-Cu systems. Strong connections and uniform distribution of observed phases comprise complement precipitation and compact microstructure and, therefore, represent the base for achieving higher

mechanical properties. Chemical composition of particular phases has been determined by EDS point analysis, as indicated at two characteristic details in Figure 6.

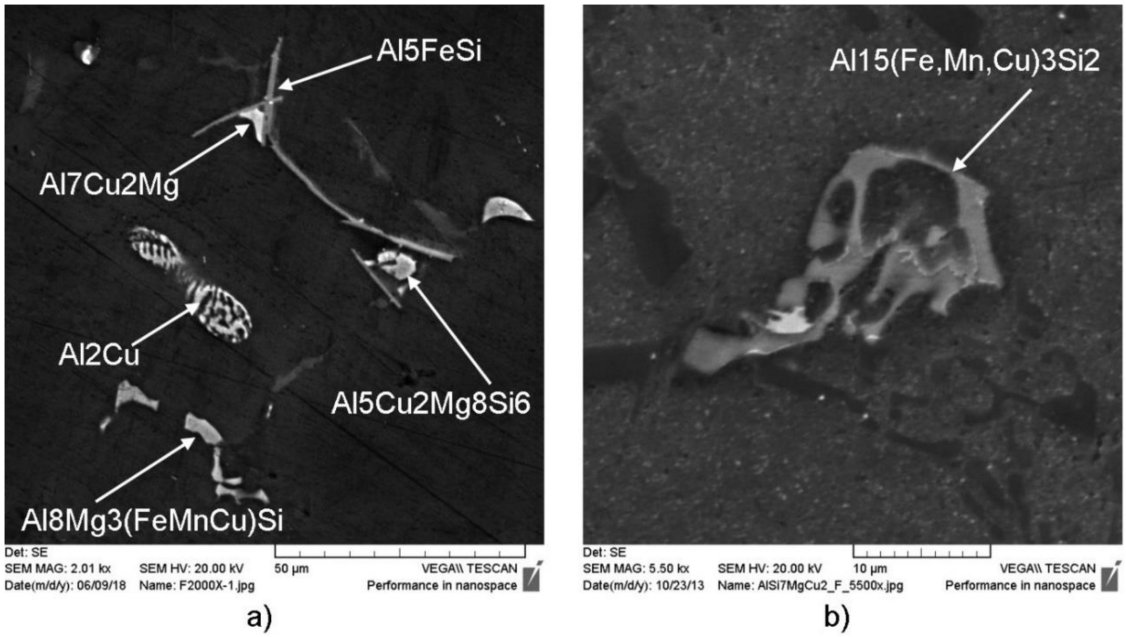

Figure 6. Microstructure of phases in AlSi7MgCu alloy: (**a**) Magnification 2000X, (**b**) Magnification 5500 X.

Quantitative chemical analysis of characteristic intermetallic phases in AlSi7MgCu alloy obtained by EDS analysis at typical intermetallic phases, shown in Figure 5, has been given as an average weight percent in Table 4.

Table 4. EDS analysis of the intermetallic compounds present in AlSi7MgCu alloy.

Element, wt.%	Al	Si	Fe	Mn	Cu	Mg
$Al_{15}(Fe,Mn,Cu)_3Si_2$	63.3	6.3	18.9	4.7	5.7	1.1
$\alpha_{Al} + \beta_{Si}$	8.7	88.6	0.5	0.4	1.3	0.6
$Al_5Cu_2Mg_8Si_6$	35.9	22.8	0.6	0.3	16.6	24.1
$Al_8Mg_3(Fe,Mn,Cu)Si$	51.5	10.6	1.1	0.5	29.7	6.0
Al_7Cu_2Mg	57.1	2.5	0.8	0.3	36.5	3.5
$Al + Al_2Cu + Si$	46.9	0.5	0.7	0.3	50.9	0.7
Matrix	95.9	-	-	-	2.4	1.7

EDS analysis indicates significant Cu presence in all present intermetallic phases. Change in chemical composition of particular phases has been noticed. Matrix (α_{Al}) and eutectic phase ($\alpha_{Al} + \beta_{Si}$) indicate high solubility of Cu. Intermetallic phases with recognizable morphology such as Chinese script ($Al_{15}(Fe,Mn,Cu)_3Si_2$) and π-phase ($Al_8Mg_3(Fe,Mn,Cu)Si$) reveal the infiltration of Cu. The amount of Cu is increasing with solidification progress. Simultaneous thermal analysis performed at heating/cooling rate at 10 K/min rate allowed further identification of significant thermodynamic changes in AlSi7MgCu alloy during the solidification process and determination of solidification sequence, as shown in Figure 7.

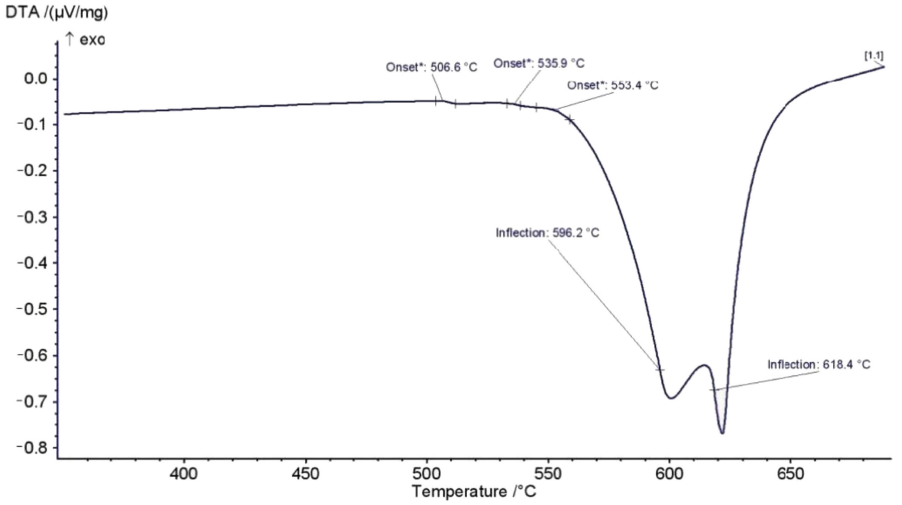

(**a**)

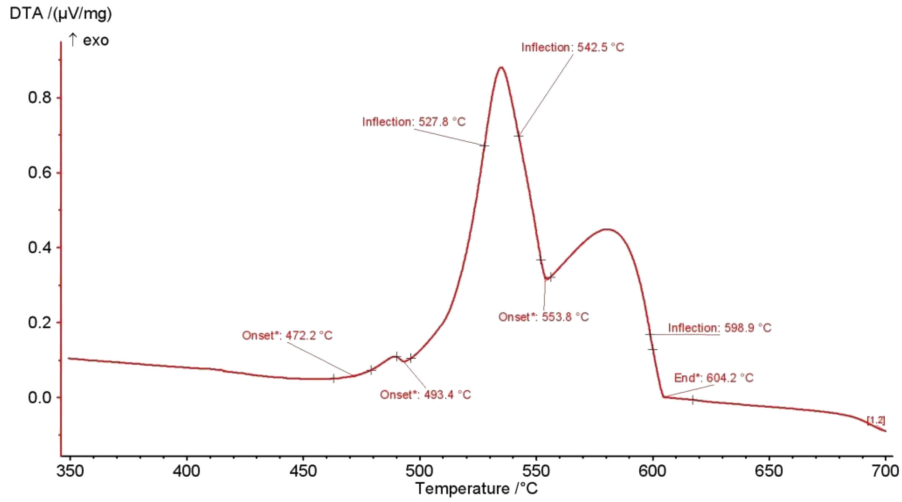

(**b**)

Figure 7. Simultaneous thermal analysis of AlSi7MgCu alloy: (**a**) heating curve, (**b**) cooling curve.

The heating and cooling curves of AlSi7MgCu alloy resulted in establishing the exact temperatures of phase transformations and precipitation, as shown in Table 5. Heating and cooling curve temperatures differ slightly due to energy output dedicated to different melting and solidification phenomena. Additionally, the heating curve did not indicate energy changes connected to all phases identified by microstructural analysis. The only strong signal related to phase transition was detected at liquidus temperature corresponding to dendrite network development. Other signals were diffused, indicating the strong interaction of a number of elements during the solidification process. Comparison of the solidification path predicted based on the equilibrium phase diagram modelling with those from simultaneous thermal analysis and microstructural investigations allowed the solidification sequence determination of AlSi7MgCu alloy listed in Table 5.

Table 5. Solidification sequence of AlSi7MgCu alloy.

Reaction Description	Reaction	$T_{heating}$, °C	$T_{cooling}$, °C
Liquidus temperature, T_l	$L \rightarrow L_1 + \alpha_{Al}$	618.4	604.2
Precipitation of high-temperature Fe-bearing phases, T_1	$L_1 \rightarrow L_3 + Al_5SiFe + Al_{15}(Fe,Mn,Cu)_3Si_2$	596.2	598.9
Eutectic temperature, T_e	$L_3 \rightarrow L_4 + (\alpha_{Al}+\beta_{Si})$	553.4	553.8
Precipitation of secondary intermetallic phases temperature, T_1	$L_4 \rightarrow L_5 + Al_8Mg_3(Fe,Mn,Cu)Si_6$	-	542.5
Precipitation of secondary intermetallic phases temperature, T_2	$L_5 \rightarrow L_6 + Al_5Cu_2Mg_8Si_6$	535.9	527.8
Precipitation of secondary intermetallic phases temperature, T_3	$L_5 \rightarrow L_6 + Al_7Cu_2Mg$	-	493.3
Precipitation of secondary intermetallic eutectic, Solidus temperature, T_s	$L_4 \rightarrow \alpha_{Al} + Al_2Cu + \beta_{Si}$	506.6	472.2

After dendrite network development, needle-like Al_5FeSi and complex Chinese script formation $Al_{15}(Fe,Mn,Cu)_3Si_2$ enriched in Cu develop from the bulk melt. The corresponding amount of Cu and Mg form metal matrix solid solution, while the complex intermetallic phases, such as $Al_8Mg_3(Fe,Mn,Cu)Si_6$ also enriched in Cu, followed by $Al_5Cu_2Mg_8Si_6$ and Al_7Cu_2Mg, cohesively precipitate from the bulk melt. Solidification ends with secondary eutectic $\alpha_{Al} + Al_2Cu + \beta_{Si}$. Dense distribution of fine complex intermetallic phases mainly with ramified morphology comprehends to the matrix coherency and also rigidity. The XRD technique was used for additional determination of the phases present in AlSi7MgCu alloys, as shown in Figure 8.

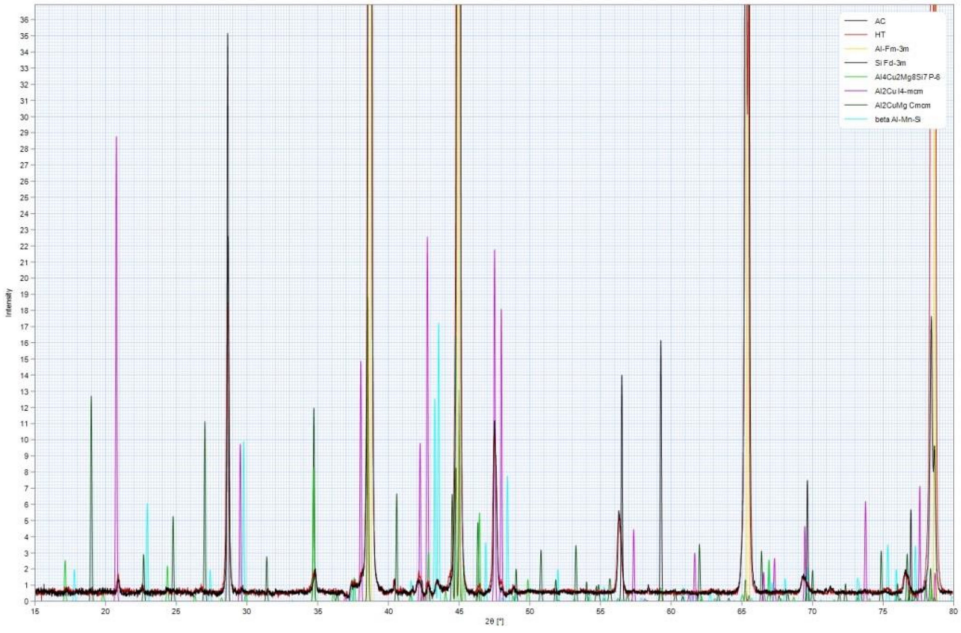

Figure 8. XRD patterns of bulk AlSi7MgCu alloy.

Complex interaction of elements and the number of particular phases indicated some difference in determined phases. XRD analysis reveals the presence of α-Al, β-Si, Al_2Cu, Al_2CuMg, $Al_4Cu_2Mg_8Si_7$, and Al-Mn-Si phases. Ratio of other present complex intermetallic phases was undetectably low.

Mechanical properties of AlSi7MgCu alloy have been investigated in order to determine the influence of higher amount of Cu and, therefore, altered the solidification sequence of an alloy. Comparison of tensile strength obtained for new AlSi7MgCu and previously investigated conventional AlSi7Mg [38] is shown in Table 6 with indicated measurement uncertainty.

Table 6. Tensile mechanical properties of AlSi7MgCu and commercial AlSi7Mg alloy in as-cast state.

Alloy	$R_{p0.2}$, MPa	R_m, MPa	A_{50}, %
AlSi7MgCu	145.8 ± 0.32%	238 ± 0.32%	3.5 ± 0.27%
AlSi7Mg	120 ± 0.32%	165 ± 0.32%	6.3 ± 0.27%

A comparison of obtained results including standard deviation data as a result of measurement dispersion and example of obtained stress–strain diagram are presented in Figure 9.

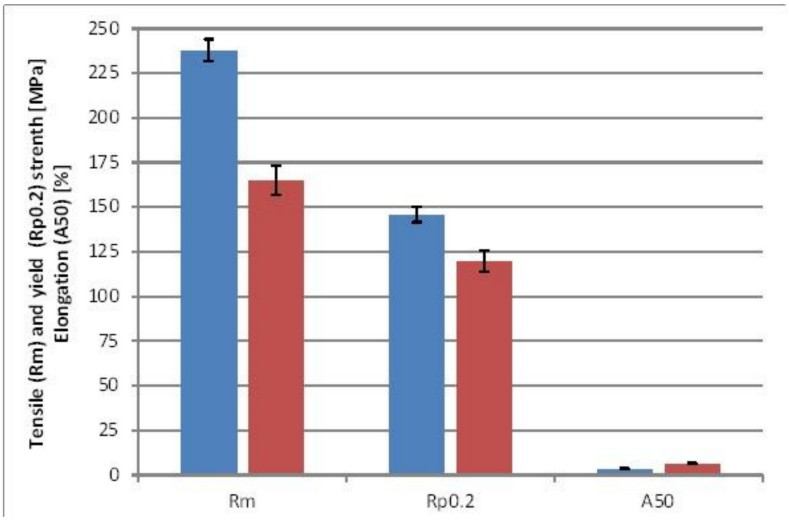

(**a**)

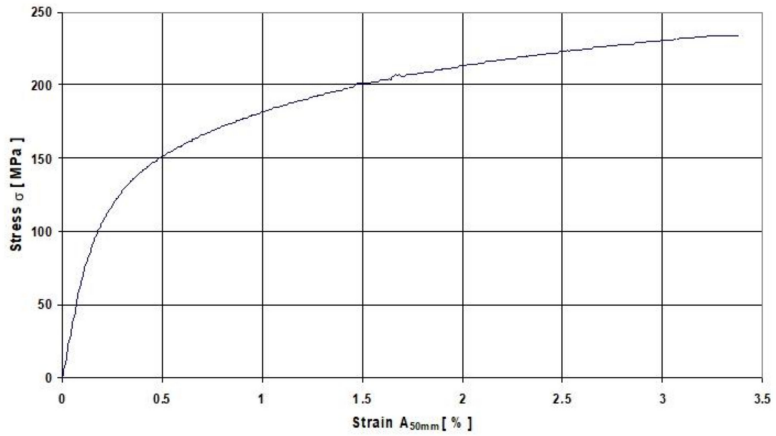

(**b**)

Figure 9. Tensile strength investigation: (**a**) comparison of tensile strength investigation for AlSi7MgCu and AlSi7Mg alloy, (**b**) an example of stress—strain curve for AlSi7MgCu alloy.

Significant increase in yield strength and tensile strength of innovative AlSi7MgCu alloy has been noticed. Determined intermetallic phases show more complexity in chemical composition and important role of Cu in whole solidification process. Microstructure analysis indicated number of phases and good coherency between precipitated intermetallics. Improvement of mechanical properties is related to the change in solidification mechanism due to Cu addition resulting in complex interactions of $Al_{15}(Fe,Mn,Cu)_3Si_2$ phase modified with Cu addition as well as formation of compacted $Al_5Cu_2Mg_8Si_6$ and $Al_8(Fe,Mn,Cu)Mg_3Si_6$ phases. Elongation of AlSi7MgCu alloy was decreased, which confirms

the rigid effect of complex intermetallic phases enriched on Cu. A densely developed microstructure with a number of fine complex intermetallic phases comprehended to obtaining higher values of tensile strength already in an as-cast state. The characterization of the solidification path for a new AlSi7MgCu alloy with high Cu content (1.435 wt.%) and correlation with obtained mechanical properties is essentially important for the automotive industry. Beside light-weighting and higher mechanical properties of automotive parts obtained already in an as-cast state, avoiding expensive heat treatment plays an important role in economic production.

4. Discussion

The design of an innovative chemical composition was based on classic composition of commercial AlSi7Mg alloy according to the EN norm. The addition of a higher amount of Cu resulted in its increase to 1.436 wt.% in the chemical composition of the alloy.

Introduction of additional amount of Cu revealed its significant interaction in solidification sequence especially below 528 °C. According to new chemical composition thermodynamic modelling of the phase diagram in equilibrium and non-equilibrium, the influence of Cu encourages the number of intermetallic phase developments. Phases such as $Al_5Cu_2Mg_8Si_6$, Al_7Cu_2Mg, and Al_2Cu are found responsible for the increase in tensile strength in a number of other commercial alloys. Narrow solidification interval indicates a potential of an alloy for casting of thin-walled sections.

Nevertheless, microstructure investigation revealed significant role of Cu even in early stages of solidification. The EDS investigation widened the palette of phases in which it occurs during the whole solidification process: $Al_{15}(Fe,Mn,Cu)_3Si_2$ at the begging of the solidification after dendrite network development, in intermetallic phase $Al_5Cu_2Mg_8Si_6$, $Al_8Mg_3(Fe,Mn,Cu)Si$, and Al_7Cu_2Mg developed after main eutectic reaction, and finally, in a secondary eutectic Al + Al_2Cu + Si as a last solidifying phase. Sophisticated FIB-SEM analysis performed on a determined volume allowed 3D reconstruction of microstructure and size and distribution of each phase present in AlSi7Mg alloy. FIB-SEM microstructure evaluation enables solidification sequence as follows: first to appear is dendrite network (α-Al), followed by fine, but ramified Al-(Fe-Mn-Cu)-Si phases and main eutectic. The bulk of the volume was filled with Al-Si-Mg-Cu phase and other intermetallic phases on the base of Al-Fe-Mg-Si, Al-Cu-Mg, and Al-Cu systems. Uniform distribution of observed phases and their coherency comprises complement precipitation and compact microstructure and therefore represent the base for update of properties. The impact in Supplementary Material was placed on Al-Si-Mg-Cu (red) and Al-(Fe-Mn-Cu)-Si (blue) systems due to infiltration of Cu in the early stages of the solidification phases. Behavior of all affected elements during the solidification process is shown in Figure 10.

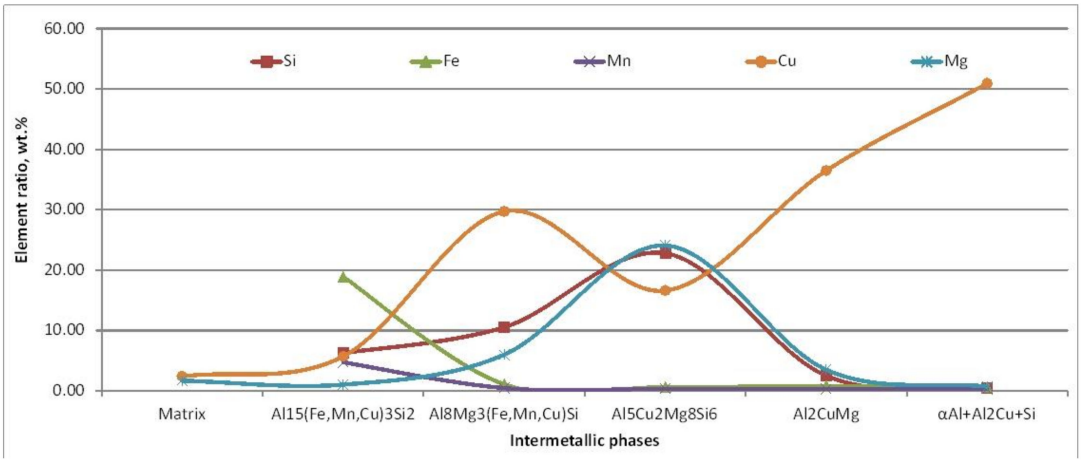

Figure 10. Elements interaction in identified phases during solidification process of AlSi7MgCu alloy.

STA analysis enabled the determination of all previously indicated phase evolution events. Due to the energy output dedicated to different melting and solidification phenomena and, therefore, overlapping of particular signals, some of the phase were identified during cooling, i.e., solidification process.

A strong connection between the microstructure constituent, XRD pattern, and characteristic temperatures of phase transformation and precipitation revealed the exact solidification sequence of AlSi7MgCu alloy.

The hypothesis of this investigation was that introduction of higher content of Cu in commercial AlSi7Mg will influence the solidification sequence change. Numerous interactions of elements and therefore phase development in innovative AlSi7MgCu alloy resulted in the diversification of microstructure development but still coherent and compact microstructure due to infiltration of Cu in intermetallic phases and high amount of Cu (1.435 wt.%) in matrix as a solid solution. The obtained microstructural constituents and their distribution due to higher Cu content had an impact on the increase in yield strength and tensile strength values already in the as-cast state, when compared to commercial AlSi7Mg alloy. Achieved improvement of mechanical properties is accomplished with the redesign of chemical composition due to Cu addition. Redesign of the microstructure manifests through complex composition of $Al_{15}(Fe,Mn,Cu)_3Si_2$ phase enriched in Cu addition as well as due to the formation of compacted $Al_5Cu_2Mg_8Si_6$ and $Al_8(Fe,Mn,Cu)Mg_3Si_6$ phases.

5. Conclusions

The investigation of redesigned innovative AlSi7MgCu alloy reveals the interaction of alloying and trace elements resulting in wide range of complex reactions and possible intermetallic phases responsible for tensile strength development. The performed investigation led to the following conclusions:

- Microstructure development and thermal analysis results allow the determination of the solidification sequence of the AlSi7MgCu alloy: dendrite network development α_{Al}, followed by common intermetallic Al_5FeSi and modified Chinese script phase in $Al_{15}(Fe,Mn,Cu)_3Si_2$ stoichiometry, main eutectic reaction $\alpha_{Al} + \beta_{Si}$ precipitation of compact complex intermetallic $Al_5Cu_2Mg_8Si_6$, Al_7Cu_2Mg, $Al_8Mg_3(Fe,Mn,Cu)Si_6$, and $\alpha_{Al} + Al_2Cu + \beta_{Si}$ phases enriched in Cu.
- Advanced microstructural investigation methods (SEM-EDS, FIB_SEM) provide an overview of the development of microconstituents and their mutual interaction
- The achieved yield and tensile strength of the investigated AlSi7MgCu alloy are significantly higher already in an as-cast state than those for common AlSi7Mg, due to favorable intermetallic phases enriched in Cu and their distribution.

The importance of achieving improved tensile strength in an as-cast state based on the understanding of solidification behavior contributes to the economically sustainable production of automotive parts.

Supplementary Materials: The following are available online at http://www.mdpi.com/2075-4701/10/12/1623/s1, Video S1: Microstructure development as a 3D distribution of Al-Si-Mg-Cu (red) and Al-(Fe-Mn-Cu)-Si (blue) phase.

Author Contributions: Conceptualization of idea, Z.Z.B. and D.S.; literature survey and comparison Z.Z.B.; design of methodology, Z.Z.B., D.S., and L.L.; experimental setup Z.Z.B. and D.S.; casting, D.S.; sample preparation, D.S. and Z.Z.B.; mechanical properties investigation, D.S.; microstructure investigation, Z.Z.B. and L.L.; STA analysis, Z.Z.B.; validation of results, Z.Z.B., D.S., and L.L.; formal analysis, Z.Z.B., D.S., and L.L.; resources, D.S. and L.L.; writing—original draft preparation, Z.Z.B.; writing—review and editing, Z.Z.B.; visualization, Z.Z.B., D.S., and L.L.; supervision, Z.Z.B. All authors have read and agreed to the published version of the manuscript.

Funding: This research received no external funding. Laboratory equipment has been provided by collaborative companies and Faculty of Metallurgy within research project IP-124 University of Zagreb Faculty of Metallurgy, Centre for Foundry Technology—SIMET, KK.01.1.1.02.0020 and VIRTULAB—Integrated laboratory for primary and secondary raw materials, KK.01.1.1.02.0022.

Acknowledgments: Investigations have been performed in collaboration with companies CIMOS-P.P.C. Buzet, d.o.o., Buzet, Croatia and FEI Netherlands, Eindhoven, The Netherlands. Investigations were performed within the Institutional project IP-124 funded by University of Zagreb Faculty of Metallurgy, topic "Design and Characterization of Innovative Engineering Alloys", Infrastructural scientific project: Centre for Foundry Technology—SIMET, KK.01.1.1.02.0020 funded by European Regional Development Fund, Operational Programme Competitiveness and Cohesion 2014–2020, and Infrastructural Scientific Project: VIRTULAB—Integrated laboratory for primary and secondary raw materials, KK.01.1.1.02.0022 funded by European Regional Development Fund, Operational Programme Competitiveness and Cohesion 2014–2020.

Conflicts of Interest: The authors declare no conflict of interest.

References

1. Raghavan, V. Al-Fe-Mn-Si (Aluminum-Iron-Manganese-Silicon). *J. Phase Equilibria Diffus.* **2007**, *28*, 215–217. [CrossRef]
2. Tillova, E.; Chalupova, M.; Hurtalova, L. Evolution of Phases in a Recycled Al-Si Cast Alloy During Solution Treatment. In *Scanning Electron Microscopy*; Kazmiruk, V., Ed.; IntechOpen: London, UK, 2012; Volume 21, pp. 411–438.
3. Tanski, T.; Labisz, K.; Krupińska, B.; Krupiński, M.; Król, M.; Maniara, R.; Borek, W. Analysis of crystallization kinetics of cast aluminum–silicon alloy. *J. Therm. Anal. Calorim.* **2015**, *123*, 63–74. [CrossRef]
4. Iqbal, N.; Van Dijk, N.; Offerman, S.; Geerlofs, N.; Moret, M.; Katgerman, L.; Kearley, G. In situ investigation of the crystallization kinetics and the mechanism of grain refinement in aluminum alloys. *Mater. Sci. Eng. A* **2006**, *416*, 18–32. [CrossRef]
5. Chang, K.; Liu, S.; Zhao, D.; Du, Y.; Zhou, L.; Chen, L. Thermodynamic description of the Al–Cu–Mg–Mn–Si quinary system and its application to solidification simulation. *Thermochim. Acta* **2011**, *512*, 258–267. [CrossRef]
6. Heugue, P.; Larouche, D.; Breton, F.; Massinon, D.; Martinez, R.; Chen, X.-G. Precipitation Kinetics and Evaluation of the Interfacial Mobility of Precipitates in an AlSi7Cu3.5Mg0.15 Cast Alloy with Zr and V Additions. *Metals* **2019**, *9*, 777. [CrossRef]
7. Dahle, A.; Arnberg, L. Development of strength in solidifying aluminium alloys. *Acta Mater.* **1997**, *45*, 547–559. [CrossRef]
8. Davis, J.R. (Ed.) *ASM Specialty Handbook: Aluminum and Aluminum Alloys*; ASM International: Ohio, OH, USA, 1993.
9. Bäckerund, L.; Chai, G.; Tamminen, J. *Solidification Characteristics of Aluminium Alloys: Foundry Alloys*; AFS/Skanaluminium: Stockhlom, Sweden, 1999; Volume 2.
10. Dispinar, D.; Campbell, J. Effect of melting and casting conditions on aluminium metal quality. *Foundry Trade J.* **2006**, *180*, 328–331.
11. Santos, J.; Dahle, A.K.; Jarfors, A.E. Magnesium Solubility in Primary α-Al and Heat Treatment Response of Cast Al-7Si-Mg. *Metals* **2020**, *10*, 614. [CrossRef]
12. McGregor, R.R. Structure and Properties. *Ind. Eng. Chem.* **1954**, *46*, 2323–2325. [CrossRef]
13. Belov, N.A.; Eskin, D.G.; Aksenov, A.A. *Multicomponent Phase Diagrams, Applications for Commercial Aluminum Alloys*; Elsevier: London, UK, 2005.
14. Brodarac, Z.Z.; Unkic, F.; Medved, J.; Mrvar, P. Determination of solidification sequence of the AlMg9 alloy. *Met. Mater.* **2012**, *50*, 59–67. [CrossRef]
15. Ji, S.; Yan, F.; Fan, Z. A High Strength Aluminium Alloy for High Pressure Die Casting. In *Light Metals—The Minerals, Metals & Materials Society*; Williams, E., Ed.; John Wiley & Sons, Inc.: Hoboken, NJ, USA, 2016.
16. Bäckman, J. Processing Aspects for Improving Mechanical Properties in Aluminium Castings. Ph.D. Thesis, Linköping University, Jönköping, Sweden.
17. Wang, E.; Hui, X.; Wang, S.; Zhao, Y.; Chen, G. Improved mechanical properties in cast Al–Si alloys by combined alloying of Fe and Cu. *Mater. Sci. Eng. A* **2010**, *527*, 7878–7884. [CrossRef]
18. Brodarac, Z.; Dolic, N.; Unkic, F. Influence of copper content on microstructure development of AlSi9Cu3 alloy. *J. Min. Met. Sect. B Met.* **2014**, *50*, 53–60. [CrossRef]

19. Samuel, F.H.; Samuel, A.M.; Doty, H.W. Factors controlling the type and morphology of Cu-containing phases in 319 Al alloy. *AFS Trans.* **1996**, *104*, 893–901.
20. Schöbel, M.; Baumgartner, G.; Gerth, S.; Bernardi, J.; Hofmann, M. Microstresses and crack formation in AlSi7MgCu and AlSi17Cu4 alloys for engine components. *Acta Mater.* **2014**, *81*, 401–408. [CrossRef]
21. Pabel, T.; Bozorgi, S.; Kneissl, C.; Faerber, K.; Schumacher, P. Hot cracking susceptibility of AlSi7MgCu alloys and effects of alloying elements magnesium and copper. *China Foundry* **2013**, *10*, 69–74.
22. Huter, P.; Oberfrank, S.; Grün, F.; Stauder, B. Thermo-mechanical fatigue influence of copper and silicon on hypo-eutectic Al–Si–Cu and Al–Si–Mg cast alloys used in cylinder heads. *Int. J. Fatigue* **2016**, *88*, 142–155. [CrossRef]
23. Huter, P.; Renhart, P.; Oberfrank, S.; Schwab, M.; Grün, F.; Stauder, B.J. High- and low-cycle fatigue influence of silicon, copper, strontium and iron on hypo-eutectic Al–Si–Cu and Al–Si–Mg cast alloys used in cylinder heads. *Int. J. Fatigue* **2016**, *82*, 588–601. [CrossRef]
24. Huter, P.; Winter, G.; Schwab, M.; Renhart, P.; Oberfrank, S.; Grün, F.; Stauder, B.J. Comparison of microstructural crack paths between hypo-eutectic Al–Si–Cu and Al–Si–Mg cast alloys in high plasticity regimes under rotating bending. *Mater. Sci. Eng. A* **2014**, *618*, 578–585. [CrossRef]
25. Dietz, S.; Djurdjevic, M.B.; Gutiérrez, R.F.; Rafetzeder, M. Solidification Path of NemAlloy. In *Vehicle and Automotive Engineering 2: Proceedings of the 2nd VAE2018 Miskolc Hungary*; Jarmai, K., Bollo, B., Eds.; Springer: Cham, Switzerland, 2018; pp. 209–219. [CrossRef]
26. Cáceres, C.; Djurdjevic, M.B.; Stockwell, T.; Sokolowski, J. The effect of Cu content on the level of microporosity in Al-Si-Cu-Mg casting alloys. *Scr. Mater.* **1999**, *40*, 631–637. [CrossRef]
27. Shabestari, S.; Moemeni, H. Effect of copper and solidification conditions on the microstructure and mechanical properties of Al–Si–Mg alloys. *J. Mater. Process. Technol.* **2004**, *153*, 193–198. [CrossRef]
28. Dugić, I.; Henriksson, F.; Strebel, C.; Kosmaz, Ö; Seifeddine, S. On the Effect of Alloying Element Range on the Mechanical Properties of Recycled Aluminium Alloy EN AB-46000. In *Light Metals 2016—The Minerals, Metals & Materials Society*; Williams, E., Ed.; John Wiley & Sons, Inc.: Hoboken, NJ, USA, 2016.
29. Zamani, M.; Seifeddine, S.; Ghassemali, E. Effect of cooling rate and eutectic modification on texture and grain structure of Al-Si-Cu-Mgdie cast alloy. *Metall. Ital.* **2016**, *108*, 29–32.
30. Tocci, M.; Pola, A.; Raza, L.; Armellin, L.; Afeltra, U. Optimization of heat treatment parameters for a nonconventional Al-Si-Mg alloy with Cr addition by DoE method. *Metall. Ital.* **2016**, *108*, 141–144.
31. Brodarac, Z.Z.; Grgurić, T.H.; Burja, J. Thermodynamic stability of AlSi11 alloy microconstituents. *J. Therm. Anal. Calorim.* **2016**, *127*, 431–438. [CrossRef]
32. Djurdjevic, M.B.; Huber, G.; Odanovic, Z. Synergy between thermal analysis and simulation. *J. Therm. Anal. Calorim.* **2012**, *111*, 1365–1373. [CrossRef]
33. Mahfoud, M.; Rao, A.K.P.; Emadi, D. The role of thermal analysis in detecting impurity levels during aluminum recycling. *J. Therm. Anal. Calorim.* **2010**, *100*, 847–851. [CrossRef]
34. Zuo, L.; Ye, B.; Feng, J.; Kong, X.; Jiang, H.; Ding, W. Effect of Q-Al 5 Cu 2 Mg 8 Si 6 phase on mechanical properties of Al-Si-Cu-Mg alloy at elevated temperature. *Mater. Sci. Eng. A* **2017**, *693*, 26–32. [CrossRef]
35. EN 1706:2010. *Aluminum and Aluminum Alloys—Castings—Chemical Compositions and Mechanical Properties*; CEN—European Committee for Standardization: Brussels, Belgium, 2010.
36. IDM 4234. *Honeywell—Garret, Industrial Division Specification, Aluminium Alloy Castings 356-F*; Garrett Motion France SAS: Thaon Les Vosges, France, 2008.
37. Stanić, D.; Zovko Brodarac, Z.; Unkić, F. Mikrostrukturna i mehanička svojstva kokilno lijevanih uzoraka AlSi7Mg legure (Microstructure and mechanical properties of AlSi7Mg alloy samples cast in permanent mould, in Croatian). In *Proceedings Book of 9th International Foundrymen Conference*; Unkić, F., Ed.; University of Zagreb Faculty of Metallurgy: Sisak, Croatia, 2009; CD_ROM 17-2009.
38. EN 10002-1:2001. *Metallic Materials—Tensile Testing—Part 1: Method of Test (at Ambient Temperature)*; CEN—European Committee for Standardization: Brussels, Belgium, 2001.
39. Zovko Brodarac, Z.; Stanić, D.; Holjevac Grgurić, T. Solidification sequence of innovative AlSi7MgCu alloy. In Proceedings of the 48th International October Conference on Mining and Metallurgy, Belgrade, Serbia, 28 September–1 October 2016; Štrbac, N., Živković, D., Eds.; University of Belgrade Technical Faculty in Bor: Zaječar, Serbia, 2016; pp. 375–378.

40. Zovko Brodarac, Z.; Stanić, D.; Li, L. Study of AlSi7MgCu alloy with improved properties in as-cast state. In Proceedings of the 73rd World Foundry Congress "Creative Foundry", Krakow, Poland, 23–27 September 2018; Sobczak, N., Asthana, R., Szajnar, J., Eds.; World Foundry Organization Ltd: Herefordshire, UK, 2018; p. 39.
41. Stanić, D.; Zovko Brodarac, Z.; Li, L. Influence of Microstructure Development on Mechanical Properties of AlSi7MgCu Alloy. In *Light Metals 2019—The Minerals, Metals & Materials Series*; Chesonis, C., Ed.; Springer: Cham, Switzerland, 2019; pp. 199–207. [CrossRef]